Synthesis, Characterization, and Application of Zr,S Co-doped TiO_2 as Visible-light Active Photocatalyst

Sun Woo Kim, Romana Khan, Tae-Jeong Kim,* and Wha-Jung Kim†

*Department of Applied Chemistry, Kyungpook National University, Daegu 702-701, Korea. *E-mail: tjkim@knu.ac.kr*
†School of Architecture, Kyungpook National University, Daegu 702-701, Korea
Received March 27, 2008

A series of Zr,S co-doped TiO_2 were synthesized by a modified sol-gel method and characterized by various spectroscopic and analytical techniques. The presence of sulfur caused a red-shift in the absorption band of TiO_2. Co-doping of sulfur and zirconium (Zr-TiO_2-S) improves the surface properties such as surface area, pore volume, and pore diameter and also enhances the thermal stability of the anatase phase. The Zr-TiO_2-S systems are very effective visible-light active catalysts for the degradation of toluene. All reactions follow pseudo first-order kinetics with the decomposition rate reaching as high as 77% within 4 h. The catalytic activity decreases in the following order: Zr-TiO_2-S > TiO_2-S > Zr-TiO_2 > TiO_2 ≈ P-25, demonstrating the synergic effect of co-doping with zirconium and sulfur. When the comparison is made within the series of Zr-TiO_2-S, the catalytic performance is found to be a function of Zr-contents as follows: 3 wt % Zr-TiO_2-S > 0.5 wt % Zr-TiO_2-S > 5 wt % Zr-TiO_2-S > 1 wt % Zr-TiO_2-S. Higher calcination temperature decreases the reactivity of Zr-TiO_2-S.

Key Words : Zr,S-doping, TiO_2, Visible light photocatalyst, Toluene decomposition

Introduction

Since Honda and Fujishima first reported a TiO_2-photo-assisted electrochemical splitting of water in 1972,[1] semiconductor photocatalysts have received a great deal of attention from both academic and industrial communities. In particular, nanocrystalline TiO_2 photocatalysts have attracted extensive interest as promising materials in view of its applications in environmental pollution control and energy storage.[2-6] However, TiO_2 is only sensitive to UV light due to its large band-gap energy (anatase: 3.2 eV). It is therefore necessary to modify the TiO_2 system for practical application because the whole radiant solar energy comprises of only 3-4% UV light. In this regard, a great deal of effort has recently been made to develop TiO_2-based photocatalysts sensitive to visible light for the purpose of efficient utilization of solar energy.

There are now known several approaches to improve the photocatalytic activity of TiO_2 materials under visible light irradiation. Some representative examples are as follows: (1) doping with metal or non-metal ions,[7-10] (2) surface modification,[11,12] and (3) combination with other semiconductors.[13,14] It must be noted, however, that each of these methods has some drawbacks. The first approach, for instance, results in thermal phase instability as well as low quantum efficiency of the photoinduced charge carriers (e^-/h^+ pairs).[15] In this connection, Ikeda has reported that TiO_2 powder loaded with transition metal such as V, Cr, Fe, Co, Cu, Mo, or W exhibits the acceleration of e^-/h^+ recombination as demonstrated by femto-second pump-probe diffuse reflection spectroscopy.[16]

To avoid these problems, non-metal ions as a dopant have been employed as an alternative approach for the formation of visible light active TiO_2 photocatalysts.[17-19] Theoretical calculation has revealed that band-gap narrowing originates from the electronic perturbations caused by the change of lattice parameters and/or by the presence of the trap states within conduction and valence bands of TiO_2.[20,21]

It is interesting to note that sulfur, unlike other non-metal dopants, may exist in more than one oxidation state (S^{2-}, S^{4+} or S^{6+}) in TiO_2 depending on the synthetic conditions or the types of sulfur precursor. The photocatalytic activity still enhances regardless of the sulfur oxidation state.[17,22]

It has recently been reported that visible light activity of TiO_2 can be even further enhanced by suitable combination of metals and/or nonmetal ions.[23-26] Of various combinations, co-doping with sulfur and zirconium may draw special interest in that zirconium increases not only the surface area and the thermal stability of TiO_2 but also retards the e^-/h^+ recombination. For instance, zirconium doped TiO_2 such as ZrO_2-TiO_2 binary metal oxides[27,28] or $Ti_{1-x}Zr_xO_2$ solid solutions[29,30] have shown higher photocatalytic activity than pure TiO_2 under UV. Further, ZrO_2-modified mesoporous nanocrystalline $TiO_{2-x}N_x$ photocatalysts showed higher photocatalytic performance than $TiO_{2-x}N_x$ for the catalytic conversion of ethylene to carbon dioxide under visible light.[31] Even more recently, Zr-doped TiO_2 film prepared by atomic layer deposition has also exhibited visible light response.[32]

Intrigued by these observations and motivated by our continued effort in the search of visible light active TiO_2 photocatalysts, we have performed the synthesis of a series of Zr,S co-doped TiO_2 (Zr-TiO_2-S) using a modified sol-gel method developed by us.[33] To the best of our knowledge, there has been no report on the synthesis as well as application of Zr,S co-doped TiO_2 as a visible light active photocatalyst. In this paper are reported their synthesis, analytical and spectroscopic characterization, and catalytic application to the degradation of gas phase toluene under visible light irradiation.

Experimental Section

Materials. Tetrabutyl orthotitanate, $Ti(O\text{-}Bu)_4$, zirconium acetylacetonate, $Zr(acac)_4$ (Tokyo Chemical Industry Co., Ltd.), thiourea (Aldrich), and absolute ethanol (Merck) were used as received. All syntheses were carried out under an atmosphere of nitrogen at room temperature.

Synthesis of Zr-TiO_2-S. Nanostructured Zr-TiO_2-S catalysts with various Zr-contents were prepared initially by taking advantage of the modified sol-gel method developed by us.[33] In a typical experiment for the synthesis of 0.5 wt % Zr-TiO_2-S, to a stirring solution of $Ti(O\text{-}n\text{Bu})_4$ (21.3 mL) in EtOH (140.0 mL) was added drop wise a mixture of HCl (6.0 mL), deionized water (22.0 mL), and EtOH (70.0 mL). Simultaneously was added drop wise a mixture of $Zr(acac)_4$ (0.15 g) and thiourea (2.38 g) in EtOH (70.0 mL). After addition the reaction mixture was stirred for 24 h under RT. Then a solution of NH_4OH (1.0 M) was added drop wise until pH of the solution rose to 9.0. The gel thus formed was aged for 2 h, separated by filtration, washed thoroughly with deionized water for complete removal of chlorides. The gel was dried at 110 °C for 12 h and was ground to powder mechanically. The resulting dry powders were calcined at 450 °C or 600 °C at the rate of 1 °C/min and kept for 5 h to obtain the nanostructured 0.5 wt % Zr-TiO_2-S. Those with other Zr-contents such as 1 wt % Zr-TiO_2-S, 3 wt % Zr-TiO_2-S, and 5 wt % Zr-TiO_2-S were prepared in the same manner.

Synthesis of Zr-TiO_2, TiO_2-S, and TiO_2. These were prepared by the same method as described above, yet in the absence of thiourea and/or $Zr(acac)_4$, respectively.

Characterization. IR spectra were run on a Mattson FT-IR Galaxy 7020A spectrophotometer. The XRD patterns were acquired on a Multi-Purpose X-ray Diffractometer (X'pert PRO MRD/X'pert PRO MPD, Cu Kα, λ = 1.5406 Å) at a scan rate of $0.03^\circ\, 2\theta\, s^{-1}$. The average crystallite size was calculated according to the Scherrer's equation,

$$D = \frac{k\lambda}{B\cos\theta} \quad (1)$$

where D is the mean crystallite size, k (0.89) is the Scherrer constant, λ is the X-ray wavelength (1.5406 Å), and B is the relative value of the full-width at half-maximum (FWHM) of the (101) diffraction peak of catalysts. The content of anatase (%) was calculated according to the equation,

$$A(\%) = \frac{I_A}{I_A + 1.256 I_R} \times 100 \quad (2)$$

where A is the content of anatase, I_A is the intensity of anatase and I_R is the intensity of rutile. Raman spectra were measured on a Laser Raman spectrophotometer (model: Ramalog 9I). Nitrogen adsorption-desorption isotherms were recorded at liquid nitrogen temperature (77 K) on a Quantachrome Instrument (NOVA 2000 series), and the specific surface areas were determined by the Brunauer-Emmett-Teller (BET) method. The Barrett-Joyner-Halenda (BJH) method was used to determine the pore size distribution derived from the BJH desorption isotherms. The morphology of the samples was examined by high-resolution transmission electron microscope (HRTEM) (model: JEOL, JEM 3010) operating at 300 kV. For TEM images, a drop of dilute dispersion was deposited on a copper grid covered with a formal-carbon membrane. The diffuse reflectance UV-Vis absorption spectra (DRS) were obtained on a UV-Vis spectrophotometer (Model Shimadzu UV-2450 diffuse reflectance mode) using $BaSO_4$ as a reflectance standard. X-ray photoelectron spectra (XPS) were recorded on a VG Scientific ESCALAB 250 XPS spectrophotometer. The instrument employs a monochromated Al Kα X-ray source ($h\nu$ = 1486.6 eV), which was used at 150 W. The area of analysis was approximately 500 μm diameter for the samples analyzed. All the binding energies were referenced to the adventitious C1s peak at 284.6 eV.

Photocatalytic Degradation of Toluene. The photocatalytic activity was investigated by the photo-degradation of gaseous toluene under visible light irradiation. The photoreaction was carried out in a closed circulation reactor under ambient conditions (Figure 1). A Pyrex-glass tubular reactor with a volume of 1 L, containing the catalyst (300 ±0.5 mg) uniformly spread over the irradiation area was connected to a peristaltic pump through tubing. The gas flow rate was 320 cm^3/min. The reactor containing the catalyst was placed in a black colored glass box (30 cm × 42 cm × 27 cm) that housed a 150 W halogen lamp (OSRAM HALOLINE) with 400 nm cutoff filter. The photon flux emitted from lamp was determined actinometrically using the potassium ferrioxalate method and found to be 3.9×10^{-6} Einstein/s. The distance between the lamp and the catalyst was 15 cm. To introduce toluene for photo-degradation study, the photo-reactor was connected to a glass mixing chamber, where the temperature was fixed at 70 °C to ensure the evaporation of toluene. The total volume of the circulation reactor was 1.3 L. The concentration of toluene used in all experiments was 3.0 μL (2.54×10^{-5} M, 530 ppmv). The photo-reactor was kept in the dark until the gas concentration remained constant, which indicated that toluene resulted in the steady state between the adsorption and desorption on the catalyst surface. In order to monitor the degradation of toluene at regular interval, Gas Chromatograph (Shimadzu GC-17A, Shimadzu Corporation) equipped with a gas sampler operat-

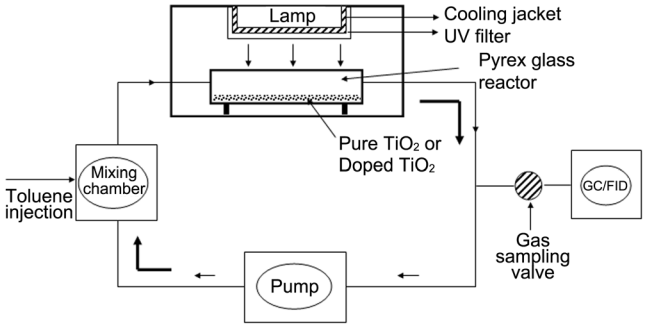

Figure 1. Schematic diagram of the photoreactor for degradation of toluene under visible light.

ing with a flame ionization detector (FID) was connected to gas exiting the reactor. The rate of degradation was estimated to obey pseudo-first-order kinetics and hence the rate constant for degradation, *k*, was obtained from the first-order plot according to equation (3),

$$\ln\frac{C_0}{C} = kt \quad (3)$$

where C_0 is the initial concentration, C is the concentration after a time (t) of the toluene degradation, and k is the first-order rate constant:

Results and Discussion

FT-IR Spectra. Figure 2 shows the FT-IR spectrum of 3 wt % Zr-TiO_2-S dried at 110 °C (Figure 2a) and of that calcined at 450 °C (Figure 2b). Some common features to be noted are the appearance of (i) broad bands below 1000 cm^{-1} assignable to the TiO_2 crystal lattice vibration[34] and (ii) those in the regions 1621-1623 cm^{-1} and 3500-3000 cm^{-1}, both being due to stretching from the hydroxyl group.[35] The deformation band (1407 cm^{-1}, Figure 2a) of ammonium ions left behind on the surface by decomposition of thiourea is absent in Figure 2b, demonstrating the effect of calcination

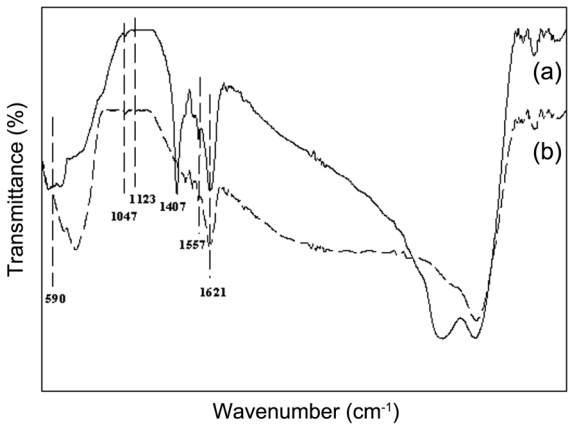

Figure 2. FT-IR spectra of 3 wt % Zr-TiO_2-S: (a) dried at 110 °C and (b) calcined at 450 °C.

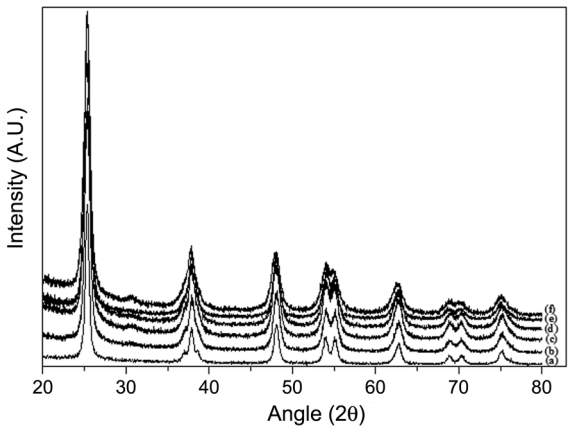

Figure 3. XRD patterns of catalysts calcined at 450 °C: (a) TiO_2, (b) TiO_2-S, (c) 0.5 wt % Zr-TiO_2-S, (d) 1 wt % Zr-TiO_2-S, (e) 3 wt % Zr-TiO_2-S, and (f) 5 wt % Zr-TiO_2-S.

at 450 °C. Yet, the weak band observed at 1557 cm^{-1} (Figure 2b) assignable to the deformation mode of C-N-H may indicate that the dissociation of thiourea is incomplete as it left a small amount in the TiO_2 lattice.[36] Finally, the Ti-S band appears at about 590 cm^{-1},[37] and the SO_4^{2-} band in the region 1047-1120 cm^{-1}.[38]

XRD Analysis. The XRD patterns of TiO_2, TiO_2-S, and x wt % Zr-TiO_2-S (x = 0.5, 1, 3, and 5) calcined at 450 °C are shown in Figure 3a-f (from bottom to top). The diffraction peaks of anatase TiO_2 can be observed in all samples (JCPDS 21-1272). Both TiO_2-S and Zr-TiO_2-S show the (101) peaks broader than that of TiO_2. These observations suggest that the lattice structure of TiO_2 is locally distorted by incorporation of dopants, S or Zr ions into TiO_2.[17,29,37] To clarify the effect of these dopants on the lattice structure of TiO_2, the lattice parameters of the catalysts were measured using (101) and (200) in anatase crystal planes by using equations 4.1 and 4.2:

$$\text{Bragg's equation: } d_{(hkl)} = \lambda/2\sin\theta \quad (4.1)$$

$$d^{-2}_{(hkl)} = h^2a^{-2} + k^2b^{-2} + l^2c^{-2} \quad (4.2)$$

where $d_{(hkl)}$ is the distance between crystal planes of (*hkl*), λ is the X-ray wavelength, θ is the diffraction angle of crystal plane (*hkl*), *hkl* is the crystal index, and *a*, *b* and *c* are lattice parameters (in anatase form, $a = b \neq c$).

The results are summarized in Table 1. The table clearly shows that the lattice parameters of all TiO_2 samples remain almost unchanged along the a- and b- axes, whereas c-axis parameter increases due to the presence of adventitious Zr and S. Ionic radius of Zr^{4+} (0.72 Å) and S^{2-} (1.7 Å) as dopants are larger than Ti^{4+} (0.61 Å) and O^{2-} (1.22 Å) in the TiO_2 structure. For possible diffusion of Zr^{4+} and S^{2-} along the c-axis to substitute Ti^{4+} or O^{2-}, respectively in TiO_2, the lattice parameters of c increase relative to that of TiO_2 because of larger ionic radius of dopants.[29,37,39] Therefore, the Zr-TiO_2-S lattice exists in a strain form with high lattice energy. Consequently, some structural defects such as oxygen vacancies might be generated on the surface of Zr-TiO_2-S.

The average crystallite size of catalysts was measured by the Scherrer's equation from the (101) peak of anatase TiO_2, and listed in Table 1. The average crystallite size of TiO_2-S (11.3 nm) or Zr-TiO_2-S (10.8-8.0 nm) is smaller than that of

Table 1. Lattice parameters and average crystallite size of Zr-TiO_2-S

Catalysts	lattice parameters (Å)[a]		Crystallite size (nm)[b]
	a = b	c	
TiO_2	3.787	9.356	14.1
TiO_2-S	3.779	9.406	11.3
0.5 wt % Zr-TiO_2-S	3.782	9.548	10.8
1 wt % Zr-TiO_2-S	3.783	9.553	9.0
3 wt % Zr-TiO_2-S	3.776	9.651	8.8
5 wt % Zr-TiO_2-S	3.782	9.499	8.0

[a]Estimated according to the equations 4.1 and 4.2. [b]Calculated according to the Scherrer formula ($D = k\lambda/B\cos\theta$).

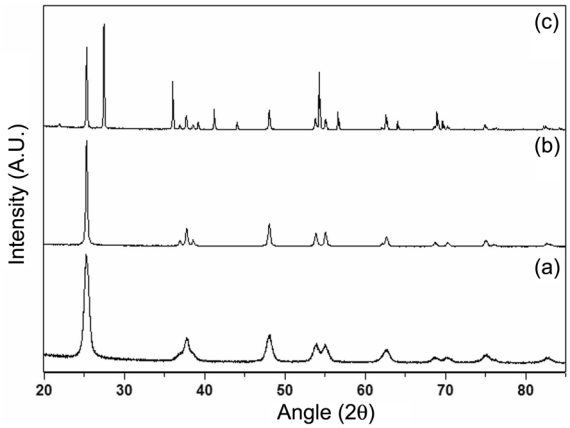

Figure 4. XRD patterns of 3 wt % Zr-TiO_2-S calcined at (a) 600 °C, (b) 800 °C and (c) 900 °C.

TiO_2 (14.1 nm). When the comparison is made within the Zr-TiO_2-S series, increase in the Zr-content decreases the size. This is because the crystallite growth in the TiO_2 lattice is suppresses as Zr or S replaces Ti^{4+} ions during the sol-gel procedure. Lattice parameters calculation confirms these observations as shown in Table 1.

Figure 4 shows the XRD patterns of 3 wt % Zr-TiO_2-S calcined at various temperatures (600, 800, and 900 °C). The anatase phase remains stable enough up to 800 °C for 5 h (Figure 4b), and undergoes transition to rutile at higher temperatures to leave 36% of anatase at 900 °C (Figure 4c). It is worth noting that the highest temperature known so far for anatase remains stable is 900 °C.[31,40,41]

Raman Spectra. Raman spectroscopy provides additional information about the anatase crystallinity. Typically TiO_2 is known to exhibit six Raman-active bands characteristic of anatase phase at 144, 197, 399, 515, 519, and 639 cm^{-1} with the symmetries of E_g, E_g, B_{1g}, A_{1g}, B_{1g}, and E_g, respectively.[42] Raman spectra of TiO_2, TiO_2-S, and 3 wt % Zr-TiO_2-S calcined at 450 °C is shown in Figure 5a-c, respectively. All spectra match quite well with those in the literature. In our hands, however, only five bands appear probably due to overlapping of A_{1g} and B_{1g} bands. At the same

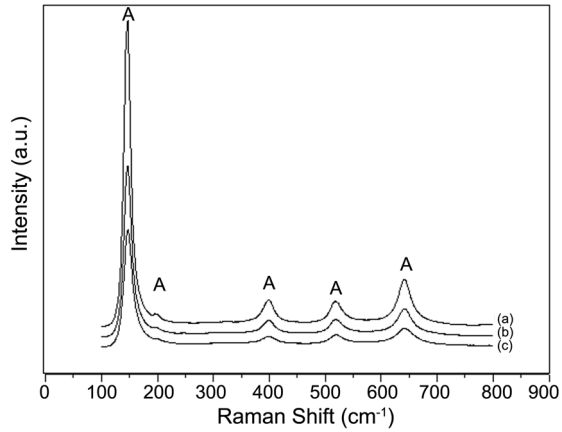

Figure 5. Raman profiles of (a) TiO_2, (b) TiO_2-S, and (c) 3 wt % Zr-TiO_2-S calcined at 450 °C (A = anatase).

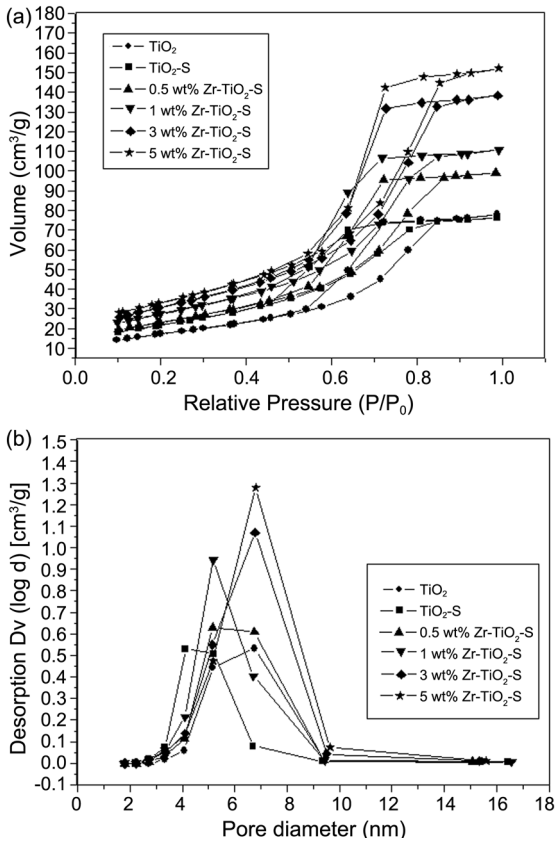

Figure 6. Textural properties of catalysts calcined at 450 °C: (a) N_2 adsorption-desorption isotherms and (b) BJH pore-size distribution curves.

time, a blue- or red-shift is accompanied for some bands, which may be explained in terms of reduction in crystallite sizes in the doped TiO_2 samples as noted earlier by others.[43] It is worth noting that reduction in the crystallite sizes has also been confirmed by the XRD measurements mentioned above.

Textural Characterization. Textural properties of catalysts calcined at 450 °C were characterized by N_2 adsorption-desorption measurements, and the corresponding data collected in Table 2. The isotherms for both undoped and doped TiO_2 clearly demonstrate mesoporosity as they belong to type IV in their behavior (Figure 6).[44] The average pore diameter of catalysts falls within the range of 3.8-6.8 nm (Table 2), and assigned to the pores among inter-aggregated particles.[45] The table also shows that the pore diameter increases with increase in the content of S as well as Zr. These observations with zirconium have some precedence in the literature. For instance, metal dopants such as Al, Zr, and Nb are known to improve the mesoporosity of TiO_2.[46] Quite interestingly, it is the first time to observe that thiourea can be employed as a pore forming agent leading to the formation of mesoporosity. In this connection, it is worth noting that urea has already been used as a pore forming agent.[47] All-in-all, Table 2 demonstrates that the modified sol-gel method involving the simultaneous co-doping of Zr and S provides greatly improved textual properties such as the surface area, the pore volume, and the pore diameter.

Table 2. Textural properties of Zr-TiO_2-S

Catalysts	BET surface area (m^2/g)[a]	BJH pore volume (cm^3/g)[b]	pore diameter (nm)[c]
TiO_2	63.37	0.12	3.80
TiO_2-S	80.08	0.13	4.11
0.5 wt % Zr-TiO_2-S	84.30	0.16	5.16
1 wt % Zr-TiO_2-S	100.4	0.18	5.17
3 wt % Zr-TiO_2-S	112.2	0.22	6.77
5 wt % Zr-TiO_2-S	120.4	0.25	6.80

[a]Measured by the BET method. [b]Taken from the volume of N_2 adsorbed at $P/P_o = 0.99$. [c]Estimated using desorption branch of the isotherm and the BJH method.

TEM Images. The TEM images of 3 wt % Zr-TiO_2-S calcined at 450 °C for 5 h in Figure 7(a) reveal the formation of mesopores due to small particle inter-aggregation. The average particle size as determined by TEM is approximately 7-8 nm, which is in good agreement with that calculated from XRD patterns. The well-resolved lattice fringes with spacing of 3.5 Å shown in Figure 7(b) demonstrate crystallinity typical of anatase TiO_2.[2,3]

UV-Visible Diffuse Reflectance Spectra (DRS). Figure 8 shows the DRS spectra of TiO_2, 3 wt % Zr-TiO_2, and 3 wt % Zr-TiO_2-S calcined at 450 °C. The figure shows that a noticeable red-shift of the optical absorption edges toward the visible region of the solar spectrum is observed only in the presence of sulfur. Therefore, one would expect band-gap narrowing in TiO_2-S and Zr-TiO_2-S to operate under visible light illumination. The band-gap energies of TiO_2, 3 wt % Zr-TiO_2, and 3 wt % Zr-TiO_2-S are 3.18, 3.17, and 3.02 eV, respectively as estimated from the equation, $E_g = 1239.8/\lambda$ where λ is the wavelength (nm) of the exciting light.[48] The figure shows further that calcination temperature also plays a role on the band-gap energy (or light-absorption property). For instance, the band-gap energy of 3 wt % Zr-TiO_2-S is smaller when calcined at 450 °C than at 600 °C (3.02 eV *vs.* 3.09 eV). Yet, the difference in energy is so small that both samples are active enough under visible light irradiation.

XPS Studies. XPS measurements were carried out to determine the chemical state of carbon, sulfur, and zirconium atoms in 3 wt % Zr-TiO_2-S calcined at 450 °C. The XPS survey spectrum in Figure 9 demonstrates the presence of titanium, oxygen, carbon, and zirconium, and at the same time the absence of sulfur. The XPS spectrum for C1*s* (Figure 10a) with a binding energy of 283-291 eV, indicating that most of carbon atoms present in the TiO_2 matrix exist as a solid solution (285 eV).[49] The small peak at 287.5 eV may be assigned to the elemental carbon originated from the traces of non-hydrolyzed alkoxy groups,[50] the residual carbon from the precursor solution,[51] and/or adventitious element carbon.[52] The binding energy of Zr 3d represents in 180-186 eV (Figure 10b). The peak at 182.2 eV corresponds to the Zr $3d_{5/2}$ state in the $Ti_{1-x}Zr_xO_2$ solid solution.[29] The absence of sulfur peak(s) on XPS explains the fact that there is no sulfur found on the surface of nanocrystals. Thus, it can be concluded that sulfur is in a high dissolution state in the TiO_2 lattice rather than an isolated oxide species on the surface of the TiO_2. The presence of sulfur was confirmed by other techniques such as elemental analysis, ICP-Mass, and EDS.

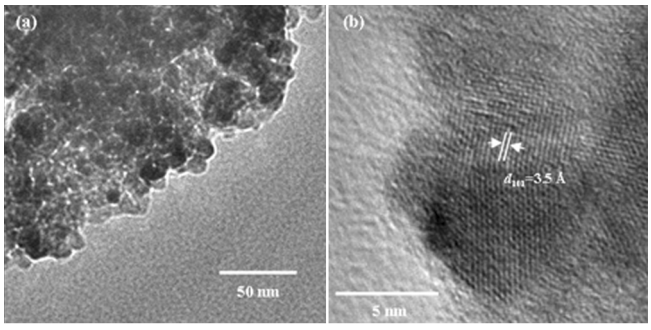

Figure 7. TEM micrograph of 3 wt % Zr-TiO_2-S calcined at 450 °C: (a) TEM image and (b) High resolution TEM image.

Photocatalytic Activity. Figure 11(a) illustrates the degradation of gaseous toluene by visible light irradiation catalyzed by TiO_2, TiO_2-S, Zr-TiO_2, and Zr-TiO_2-S calcined at 450 °C along with P-25 for comparison. All reactions exhibit pseudo first-order kinetics as illustrated in Figure 11, and relevant data summarized in Table 3. Most interestingly, it is for the first time to observe that our Zr-TiO_2-S system is quite an effective visible-light active catalyst. The degradation of toluene reaches as high as 77% within 4 h. This system exhibits much higher reactivity than any of the remaining catalysts such as TiO_2-S, Zr-TiO_2, TiO_2, and P-25. These observations suggest that co-doping with both zirconium and sulfur is more beneficial for the enhancement of catalytic efficiency than doping with sulfur or zirconium alone. Sulfur has been known to reduce the band-gap energy of TiO_2, thus for example moving the UV absorption band toward the visible region,[10,17] as is confirmed by the DRS spectra in Figure 8. This fact is also reflected in the enhanced reactivity of TiO_2-S as compared with that of 3 wt % Zr-TiO_2 or TiO_2 (Table 3). Nevertheless surface properties of catalysts were enhanced by the zirconium dopants as shown by texture properties (Table 2). Therefore, Zr-TiO_2-S has much better photocatalytic performance compared with that

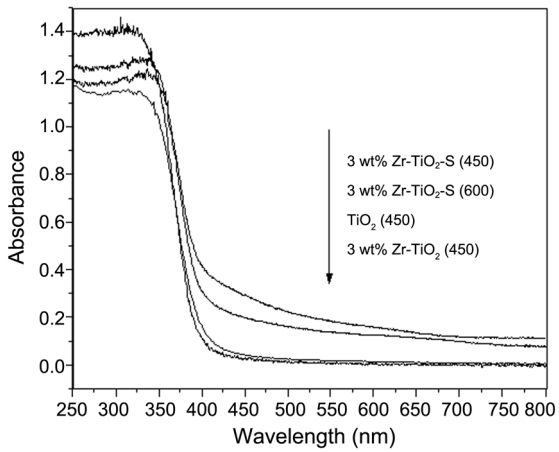

Figure 8. UV-visible diffuse reflectance spectra of TiO_2, 3 wt % Zr-TiO_2, 3 wt % Zr-TiO_2-S calcined at 450 °C, and 3 wt % Zr-TiO_2-S calcined at 600 °C.

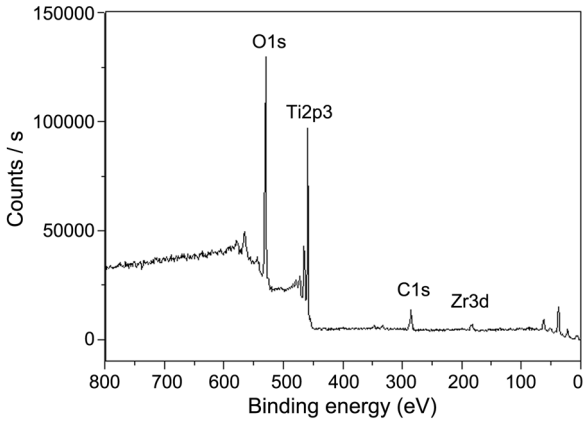

Figure 9. XPS spectrum of 3 wt % Zr-TiO_2-S calcined at 450 °C.

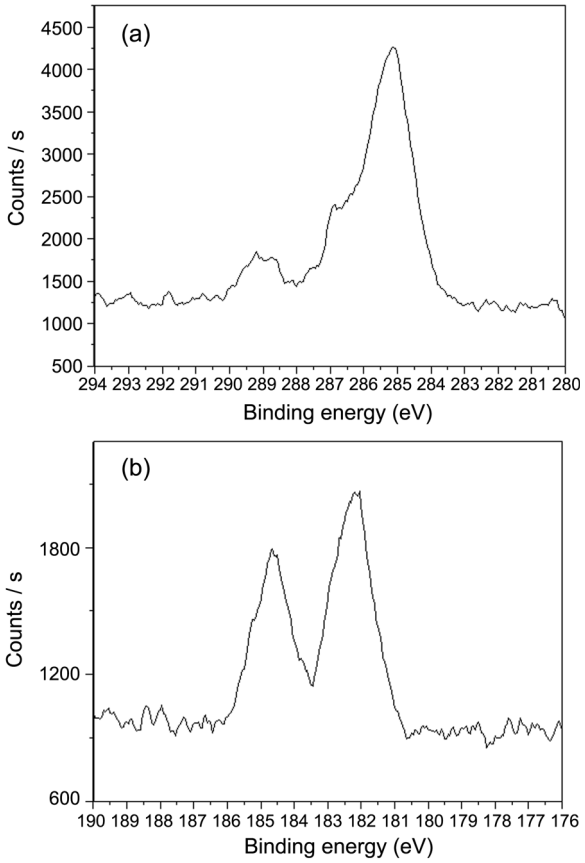

Figure 10. XPS spectra of (a) C1*s* and (b) Zr3*d* peaks.

of only sulfur doped TiO_2 (Table 3).

Higher catalytic activity with doping can be explained in the following ways. Gas-solid heterogeneous photocatalysis is a surface-based process, and therefore enhanced surface properties of catalysts have positive effects on such process.[2] In general, doping with metal inhibits the crystal growth of the catalysts so that the porous structure with high surface area can be preserved. Furthermore, some structural defects such as vacancies in lattice can be generated as dopants replace titanium and oxygen ions.[29] Some oxides (O^{2-}) being replaced from the surface may trap the photo-generated holes (h^+) to be oxidized to peroxides (O^{1-}) which in turn

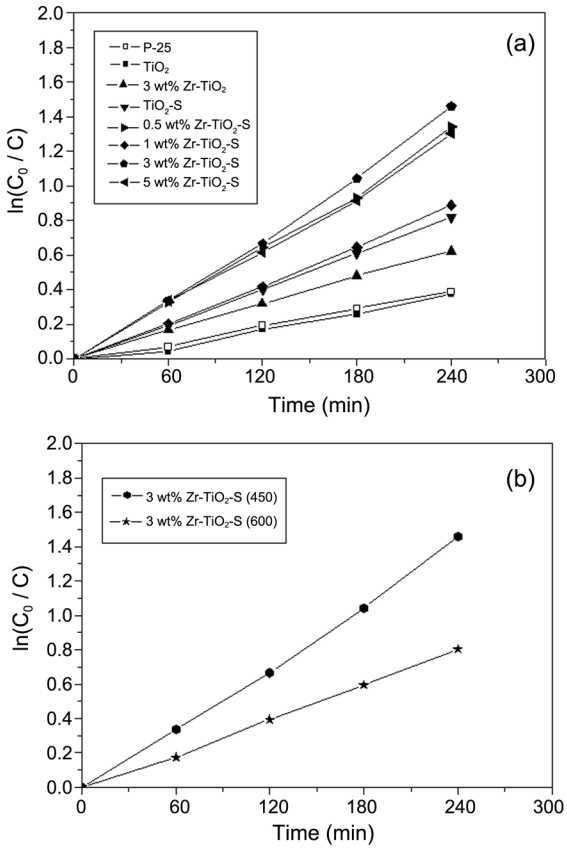

Figure 11. Photocatalytic degradation of toluene under visible light irradiation: (a) various catalysts calcined at 450 °C and (b) 3 wt % Zr-TiO_2-S calcined at 450 °C or 600 °C. C_0 = the initial concentration; C = the concentration at time t.

trap further holes (h^+) to attack as oxygen (O) the chemical bonds of surface adsorbed organic pollutants. In addition, the holes (h^+) also react with surface adsorbed water to generate hydroxyl radicals (OH), which have a powerful oxidizing power for degradation of organic pollutants.[52]

When the comparison is made within the Zr-TiO_2-S series, the reactivity decreases in the following order: 3 wt % Zr-TiO_2-S > 0.5 wt % Zr-TiO_2-S > 5 wt % Zr-TiO_2-S > 1 wt % Zr-TiO_2-S. This order indicates that there seems to be an optimum zirconium content (Zr = 3 wt %) for the highest catalytic performance. Finally, the calcination temperature also plays a role in the reactivity of Zr-TiO_2-S. A slight blue-

Table 3. Photodegradation of toluene under visible light irradiation

Catalysts	Degradation (%)[a]	k (min^{-1})[b]
P-25	32	0.001615 ± 0.0001
TiO_2	31	0.001566 ± 0.0002
3 wt % Zr-TiO_2	46	0.002589 ± 0.0003
TiO_2-S	56	0.003409 ± 0.0003
0.5 wt % Zr-TiO_2-S	74	0.005598 ± 0.0006
1 wt % Zr-TiO_2-S	59	0.0037 ± 0.0003
3 wt % Zr-TiO_2-S	77	0.006081 ± 0.0007
5 wt % Zr-TiO_2-S	73	0.005427 ± 0.0004
3 wt % Zr-TiO_2-S (600)[c]	55	0.00335 ± 0.0003

[a]Measured after reaction for 4 h. [b]Apparent rate constant calculated from the linear fitting of $\ln(C_0/C)$ *vs*. reaction time. [c]Calcined at 600 °C.

shift is observed in the DRS spectrum of 3 wt % Zr-TiO_2-S when the sample is treated at higher temperature such as 600 ^oC (Figure 8) along with decrease in the reactivity (Table 3, Figure 11b). These observations can be rationalized in terms of removal of sulfur at an elevated temperature.

Conclusions

A series of Zr-TiO_2-S were synthesized by a modified sol-gel method developed earlier by us. They were characterized by various spectroscopic and analytical techniques. Surface properties as well as thermal stability of the anatase phase are greatly enhanced by co-doping with zirconium and sulfur. The Zr-TiO_2-S systems are very effective visible-light active catalysts for the degradation of toluene. The synergic effect of co-doping with zirconium and sulfur is encountered in the catalytic performance of Zr-TiO_2-S to show the reactivity order as follows: Zr-TiO_2-S > TiO_2-S > Zr-TiO_2 > TiO_2≈P-25. Within the same series the catalytic performance is found to be a function of Zr-contents as follows: 3 wt % Zr-TiO_2-S > 0.5 wt % Zr-TiO_2-S > 5 wt % Zr-TiO_2-S > 1 wt % Zr-TiO_2-S. Higher calcination temperature decreases the reactivity of Zr-TiO_2-S.

Acknowledgements. TJK gratefully acknowledges the financial support from Korea Institute of Construction & Transportation Technology Evaluation and Planning (Grant No. C10A1000018-06A0200-01220). Dr. Jin-Ook Baeg (Korea Research Institute of Chemical Technology) is also acknowledged for DRS measurements and Prof. Chang-mo Nam (Yeongnam College of Science & Technology) for providing the photoreactor. Spectroscopic and analytical measurements were performed by KBSI and the Center for Scientific Instruments, KNU.

References

1. Fujishima, A.; Honda, K. *Nature* **1972**, *238*, 37.
2. Hoffmann, M. R.; Martin, S. T.; Choi, W.; Bahnemann, D. W. *Chem. Rev.* **1995**, *95*, 69.
3. Linsebigler, A. L.; Lu, G.; Yates Jr., J. T. *Chem. Rev.* **1995**, *95*, 735.
4. Fujishima, A.; Hashimoto, K.; Watanabe, T. *TiO_2 Photocatalysis: Fundamentals and Application*; BKC: Tokyo, 1999.
5. Takahashi, Y.; Tatsuma, T. *Langmuir* **2005**, *2*, 12357.
6. Lim, S. H.; Luo, J.; Zhong, Z.; Ji, W.; Lin, J. *Inorg. Chem.* **2005**, *44*, 4124.
7. Kim, S.; Hwang, S.-J.; Choi, W. *J. Phys. Chem. B* **2005**, *109*, 24260.
8. Wang, X. H.; Li, J.-G.; Kamiyama, H.; Moriyoshi, Y.; Ishigaki, T. *J. Phys. Chem. B* **2006**, *110*, 6804.
9. Ashi, R.; Morikawa, T.; Ohwaki, T.; Aoki, K.; Taga, Y. *Science* **2001**, *293*, 269.
10. Umebayashi, T.; Yamaki, T.; Tanaka, S.; Asai, K. *Chem. Lett.* **2003**, *32*, 330.
11. Robel, I.; Subramanian, V.; Kuno, M.; Kamat, P. V. *J. Am. Chem. Soc.* **2006**, *128*, 2385.
12. Jiang, D.; Xu, Y.; Hou, B.; Wu, D.; Sun, Y. *J. Solid State Chem.* **2007**, *180*, 1787.
13. Lettmann, C.; Hinrichs, H.; Maier, W. F. *Angew. Chem. Int. Ed. Engl.* **2001**, *40*, 3160.
14. Liu, B.; Zhao, X.; Zhang, N.; Zhao, Q.; He, X.; Feng, J. *Surf. Sci.* **2005**, *595*, 203.
15. Choi, W.; Termin, A.; Hoffmann, M. R. *J. Phys. Chem.* **1994**, *98*, 13669.
16. Ikeda, S.; Sugiyama, N.; Pal, B.; Marcí, G.; Palmisano, L.; Noguchi, H.; Uosaki, K.; Ohtani, B. *Phys. Chem. Chem. Phys.* **2001**, *3*, 267.
17. Ohno, T.; Akiyoshi, M.; Umebayashi, T.; Asai, K.; Mitsui, T.; Matsumura, M. *Appl. Catal., A* **2004**, *265*, 115.
18. Cong, Y.; Zhang, J.; Chen, F.; Anpo, M. *J. Phys. Chem. C* **2007**, *111*, 6976.
19. Ren, W.; Ai, Z.; Jia, F.; Zhang, L.; Fan, X.; Zou, Z. *Appl. Catal., B: Environ.* **2007**, *69*, 138.
20. Serpone, N. *J. Phys. Chem. B* **2006**, *110*, 24287.
21. Wang, H.; Lewis, J. P. *J. Phys.: Condens. Matter.* **2006**, *18*, 421.
22. Ho, W.; Yu, J. C.; Lee, S. *J. Solid State Chem.* **2006**, *179*, 1171.
23. Zhao, W.; Ma, W.; Chen, C.; Zhao, J.; Shuai, Z. *J. Am. Chem. Soc.* **2004**, *126*, 4782.
24. Gao, B.; Ma, Y.; Cao, Y.; Yang, W.; Yao, J. *J. Phys. Chem. B* **2006**, *110*, 14391.
25. Ohno, T.; Miyamoto, Z.; Nishijima, K.; Kanemitsu, H.; Xueyuan, F. *Appl. Catal., A* **2006**, *302*, 62.
26. Morikawa, T.; Irokawa, Y.; Ohwaki, T. *Appl. Catal., A* **2006**, *314*, 123.
27. Fu, X.; Clark, L. A.; Yang, Q.; Anderson, M. A. *Environ. Sci. Technol.* **1996**, *30*, 647.
28. Twesme, T. M.; Tompkins, D. T.; Anderson, M. A.; Root, T. W. *Appl. Catal., B: Environ.* **2006**, *64*, 153.
29. Yu, J. C.; Lin, J.; Kwok, R. W. M. *J. Phys. Chem. B* **1998**, *102*, 5094.
30. Huang, Y.; Zheng, Z.; Ai, Z.; Zhang, L.; Fan, X.; Zou, Z. *J. Phys. Chem. B* **2006**, *110*, 19323.
31. Wang, X.; Yu, J. C.; Chen, Y.; Wu, L.; Fu, X. *Environ. Sci. Technol.* **2006**, *40*, 2369.
32. Qui, S.; Starr, T. L. *J. Electrochem. Soc.* **2007**, *154*, H472.
33. Khan, R.; Kim, S. W.; Kim, T.-J.; Lee, H. S. *Bull. Korean Chem. Soc.* **2007**, *28*, 1951.
34. Zhu, Y.; Liu, T.; Ding, C. *J. Mater. Res.* **1999**, *14*, 442.
35. Cheng, P.; Qiu, J.; Gu, M.; Shangguan, W. *Mater. Lett.* **2004**, *58*, 3751.
36. Ren, L.; Huang, X.; Sun, F.; He, X. *Mater. Lett.* **2007**, *61*, 427.
37. Sun, H.; Bai, Y.; Cheng, Y.; Jin, W.; Xu, N. *Ind. Eng. Chem. Res.* **2006**, *45*, 4971.
38. Bacsa, R.; Kiwi, J.; Ohno, T.; Albers, P.; Nadtochenko, V. *J. Phys. Chem. B* **2005**, *109*, 5994.
39. Yu, J. C.; Ho, W.; Yu, J.; Yip, H.; Wong, P. K.; Zhao, J. *Environ. Sci. Technol.* **2005**, *39*, 1175.
40. Pillai, S. C.; Periyat, P.; George, R.; McCormack, D. E.; Seery, M. K.; Hayden, H.; Colreavy, J.; Corr, D.; Hinder, S. J. *J. Phys. Chem. C* **2007**, *111*, 1605.
41. Padmanabhan, S. C.; Pillai, S. C.; Colreavy, J.; Balakrishnan, S.; McCormack, D. E.; Perova, T. S.; Gun`ko, Y.; Hinder, S. J.; Kelly, J. M. *Chem. Mater.* **2007**, *19*, 4474.
42. Ohsaka, T.; Izumi, F.; Fujiki, Y. *J. Raman Spectrosc.* **1978**, *7*, 321.
43. Hamal, D. B.; Klabunde, K. J. *J. Colloid Interface Sci.* **2007**, *311*, 514.
44. Sing, K. S. W.; Everett, D. H.; Haul, R. A. W.; Moscou, L.; Pierotti, R. A.; Rouquerol, J.; Siemieniewska, T. *Pure Appl. Chem.* **1985**, *57*, 603.
45. Yu, J.; Yu, J. C.; Leung, M. K.-P.; Ho, W.; Cheng, B.; Zhao, X.; Zhao, J. *J. Catal.* **2003**, *217*, 69.
46. Kondo, J. N.; Yamashita, T.; Nakajima, K.; Lu, D.; Hara, M.; Domen, K. *J. Mater. Chem.* **2005**, *15*, 2035.
47. O'Regan, B.; Grätzel, M. *Nature* **1991**, *353*, 737.
48. Shi, Z. M.; Ye, X. Y.; Liang, K. M.; Gu, S. R.; Pan, F. *J. Mater. Sci. Lett.* **2003**, *22*, 1255.
49. Lettmann, C.; Hildenbrand, K.; Kish, H.; Macyk, W.; Maier, W. F. *Appl. Catal., B: Environ.* **2001**, *32*, 215.
50. Yu, J. C.; Yu, J. G.; Ho, W. K.; Jiang, Z. T.; Zhang, L. Z. *Chem. Mater.* **2002**, *14*, 3808.
51. Sakthivel, S.; Kisch, H. *Angew. Chem. Int. Ed.* **2003**, *42*, 4908.
52. Ollis, D. F.; Al-Ekabi, H. *Photocatalytic Purification and Treatment of Water and Air*; Elsevier: Amsterdam, 1993.